Waste Heat Recovery from Engine Coolant on Mild Hybrid Vehicle using Organic Rankine Cycle

Charbel Mansour[a], Wissam Bou Nader[b,c], Clément Dumand[c] and Maroun Nemer[b]

[a] Industrial and Mechanical Engineering department, Lebanese American University, New York, United-States, charbel.mansour@lau.edu.lb
[b] Centre Efficacité Energétique des Systèmes, Ecole des Mines de Paris, Palaiseau, France, wissam.bou_nader@mines-paristech.fr, maroun.nemer@mines-paristech.fr
[c] PSA Group, Centre technique de Vélizy, Vélizy, France, wissam.bounader@mpsa.com, clement.dumand@mpsa.com

Abstract:

Considerable efforts have been invested in the automotive industry on electrified powertrains in order to reduce passenger cars' dependence on fossil fuels. Powertrains electrification resulted in a wide range of mass-production hybrid vehicle models, ranging from micro-hybrid, to mild, full and battery-extended hybrids such as plug-in and range-extender electric vehicles. Fuel savings of these powertrains strongly rely on the energy management strategy (EMS) deployed on-board, as well as on the technology used to recover the waste heat energy. This paper investigates the fuel savings potential of a mild hybrid vehicle using an Organic Rankine Cycle (ORC) for generating electricity from the engine-coolant circuit. The net mechanical power and electrical power generated from the ORC are determined based on experimental data recorded on a 1.2-liters turbocharged engine. The coolant temperature is regulated at 85°C and 105°C depending on the engine load. The R-1234yf organic fluid is used and the Rankine operating pressure has been controlled to maximize the overall system efficiency under technological constraints. The dynamic programming control is used as a global optimal energy management strategy in order to define the best strategy for the engine operation and power-split between the electric and thermal paths of the powertrain. A sensitivity analysis is also performed to find the optimal size of the electric motor while taking into account the additional weight of the ORC system. Results show 2.4% of fuel economy improvement on the WLTC.

Keywords:
Mild Hybrid, Organic Rankine Cycle, Waste Heat Recovery, Engine-Coolant, Dynamic Programming.

1. Introduction

Several waste heat recovery (WHR) systems are being examined in the automotive industry for different applications, all serving to improve the overall vehicle efficiency. Rankine cycle, thermo-acoustic, Stirling engine, thermo-electric generator, turbo-compound and thermo-chemical recuperation are main examples of these considered WHR systems [1-12, 46]. This paper focuses on recovering engine-coolant waste heat using organic Rankine cycle (ORC). In fact, a comprehensive review on WHR systems from low temperature energy source such as the case of the engine-coolant considered in this study, shows that the ORC is the best configuration to recover the waste heat, with 20% better efficiency compared to the Trilateral Flash Cycle and 70% compared to the Kalina cycle [48].

The implementation of ORC in automotive applications has been investigated for years and relevant examples are found in the literature where energy is recovered from both heat loss sources in the internal combustion engine: the exhaust gas and/or the engine-coolant [2-5, 13]. Exhaust gas presents a high quality energy source but with a dynamic temperature profile where temperatures can fluctuate very quickly between 200°C and 800°C downstream the catalytic converter; whereas the engine-coolant presents a relatively low temperature source, however with a steady profile ranging between 85 °C and 105 °C during normal hot engine operating conditions.

The first Rankine demonstration for recovering waste heat from exhaust gas appeared on MAN commercial vehicles near the 1970 [14]. Commercialization of similar Rankine systems on these vehicles from other heavy-duty constructers is expected on the near term, with an announced fuel reductions up to 10% [15-20]. In 2014, Hino investigated the use of another type of ORC, recovering heat from the coolant circuit. The engine-coolant recovers heat first from the exhaust gas, before rejecting the heat to the organic fluid of the ORC evaporator. A fuel economy improvement of 7.5% is announced for a constant speed cruise of 80 km/h [21]; however, the system is complex for automotive application.

The main developments on Rankine systems for passenger cars are performed on exhaust gas as energy source. Honda presented the first implemented prototype in 2007 [22, 23], with an announced increase in the thermal efficiency of the internal combustion engine from 28.9% to 32.7% at constant speed of 100 km/h. In 2009, BMW presented its second turbo streamer generation, announcing a consumption gain between 3 and 5% for vehicle velocity between 70 to 150 km/h [24, 25]. Both manufacturers have investigated the potential of fuel saving with Rankine cycle recovering heat from the exhaust gas. The potential of recovering heat from the exhaust with water as working fluid was investigated by IFPEN in 2011. Tests were performed on a gasoline engine, and a net mechanical power of 1 kW was recovered at 130 km/h, which correspond to 3.1% of the engine power at this operating point [26, 27].

Comparison of ORC applications showed better results with commercial vehicles compared to passenger cars because the formers operate typically at higher loads, and therefore at higher exhaust gas temperatures, where waste heat recovery potential is considerable. Therefore, vehicle manufacturers have focused the developments on ORC systems for exhaust gas waste heat recovery. However, it is noteworthy to mention that the advantage of ORC systems using the engine-coolant as energy source is the pseudo constant temperature of the water coolant, which ranges between 85 °C and 105 °C [21]. Thus, the ORC system components can be better optimized to maximize the heat recovery, namely the evaporator.

Therefore, based on the above synthesis of the insights and gaps in the literature for adopting ORC systems for waste heat recovery from engine-coolant in passenger cars, this study proposes a comprehensive methodology to assess these systems on a mild hybrid vehicle. This vehicle configuration is considered given the rising interest of vehicle manufacturers in low-level powertrain electrification, in addition to the reliance of the vehicle on the engine as prime mover for traction, which makes the waste heat recovery from the engine-coolant desirable. This is unlike the case of full hybrid vehicles where the engine stops frequently and the vehicle can be driven in electric mode over considerable part of the trip [49].

The ORC system description and power recovery potential are investigated in section 2, using the R-1234yf working fluid. This section presents as well a methodology for maximizing the ORC overall efficiency in order to maximize the heat recovery from the coolant while avoiding any disruption in the engine normal operation. Section 3 presents a detailed modeling of the mild hybrid powertrain and the optimal sizing of the starter-alternator, while considering the ORC weight. The energy management strategy of the powertrain is presented in this section as well using dynamic programming. Section 4 discusses the obtained results on fuel saving potential under the NEDC and the WLTC.

2. Organic Rankine cycle model

2.1. System description

Internal combustion engines require an efficient and properly sized cooling system in order to preserve the engine life and provide the adequate operating conditions. A considerable rate of the heat generated in the combustion chamber that was not converted into mechanical work on the piston is removed, with an adjustable evacuation rate according to the engine operating temperature. This prevent the excessive heat removal, which deteriorates the engine thermal efficiency and reduces engine longevity. Figure 1 illustrates (in black) a typical water-cooling system in a passenger car, where the undesired waste heat from the combustion chamber and the oil-lubricant is removed by the coolant, and rejected into the ambient air through the radiator. Then, the cooled engine-coolant flows back into the engine. Part of the hot coolant is bypassed through a cabin heater unit for ensuring thermal comfort during cold climates. Note that during cold engine operation, a thermostat valve closes the engine outlet channel and the coolant circulates only throughout the engine block in order to accelerate the warm-up process.

For the scope of this study, the engine warm-up and cabin heating are not considered; therefore, recovering part of the coolant waste heat with an ORC is assumed for a warm engine operating at nominal rated temperature. The engine temperature is regulated to operate at two different values as observed from conducted test bench measurements on the considered engine: at high engine load (over 50%) the engine-coolant temperature is regulated to 85°C, and at low to mid-load (below 50%) the coolant temperature is regulated to 105°C. In fact, at high load, a deflector placed on the radiator is actuated in order to increase the amount of air that cools the engine-coolant in the radiator at the expense of slightly deteriorating the vehicle drag coefficient. This leads to decreasing the coolant temperature to 85°C. This safety measure is considered by the thermal-management control unit of the engine to preserve it from high thermo-mechanical stresses, in case the vehicle suddenly stops when preceded by a long drive at high load. The engine temperature in this case will rise and can cause engine failure. Thus, the engine-coolant in this study is regulated to operate at either 85°C or 105°C, depending on the engine operating point, even during engine transient operation. This is one the main advantages of the suggested ORC system, which is to recover heat from a constant temperature energy source (either at 85 or 105) where the system components can be optimized to maximize the heat recovery, unlike the case of recovery form waste exhaust gas.

The ORC is also illustrated in Figure 1 (in green), consisting of a pump, an evaporator, a turbine and a condenser. The working fluid undergoes four consecutive thermodynamic processes: (1-2) an adiabatic pressurization in the pump, (2-3) an isobaric heat recovery from the engine-coolant in the evaporator, (3-4) an adiabatic expansion in the turbine and (4-1) an isobaric heat rejection to the ambient air in the condenser. The system produces mechanical work from expanding the working fluid in the turbine while exchanging heat between the hot engine-coolant (energy source) and the ambient air (cold sink). The produced mechanical work is used to generate electricity and store it in the battery of a mild hybrid vehicle, presented in section 3.

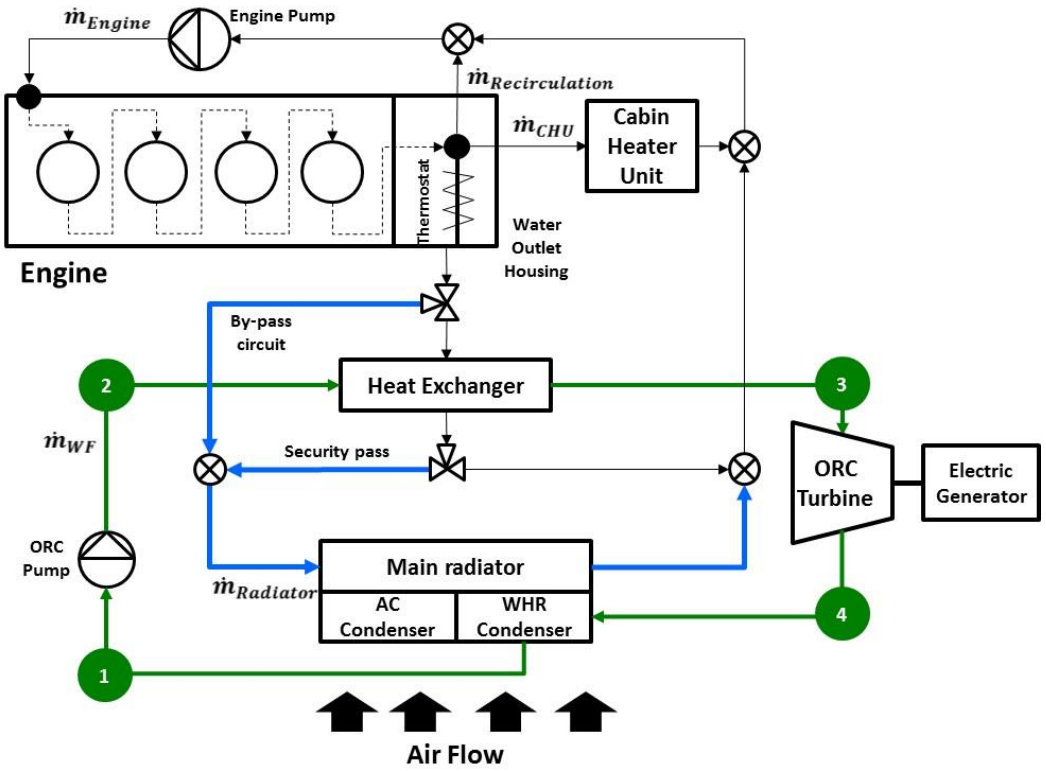

Fig. 1. Cooling system and ORC system on thermal engine.

2.2. Working fluid selection

The considered working fluid is the R-1234yf, an organic isentropic fluid that offers thermo-physical properties similar to the currently used R-134a in automotive applications, and used currently as a substitute to the R-134a in the European vehicle fleet mobile air conditioners [28]. It presents several advantages at different levels. On the one hand, R-1234yf presents a remarkably environmental performance with a null ozone depletion potential and a low global warming potential (GWP=4). Moreover, it presents low implementation complexity for Rankine cycle and it is capable of recovering some of the engine-coolant heat at temperatures between 85°C and 105°C during normal operations, as it evaporates at temperatures close to these with a relatively high pressure, unlike other working fluids that evaporates at higher temperatures. On the other hand, another major drive for using the R-1234yf is its isentropic type characteristic; thus, it provides the ability to avoid diphasic expansion (3-4) unlike the case of wet working fluids such as water, which requires overheating from the saturated vapor state to avoid two-phase state at the end of the expansion. This makes the R-1234yf an appropriate working fluid candidate for the use of a turbine expansion machine instead of the costly piston machines, typically used in ORC [29-31].

2.3. Power recovery potential from the coolant using ORC

This section determines the potential mechanical power ($\dot{W}_{net}$) to be recovered using the ORC, which is represented as the product resultant of the coolant thermal capacity from the radiator ($\dot{Q}_{radiator}$) and the overall efficiency of the considered heat recovery system ($\eta_{overall}$), as shown in equation (1). Thus, in order to maximize $\dot{W}_{net}$, the overall recovery efficiency is optimized at each engine operating point. This section investigates both the thermal capacity potential and the overall efficiency of the recovery system. It also presents an optimization methodology for the efficiency.

$$\dot{W}_{net} = \eta_{overall} \times \dot{Q}_{radiator} \quad (1)$$

2.3.1. Thermal capacity potential of the coolant in the radiator

In order to design the ORC system, it is necessary to evaluate the potential waste heat of the coolant dissipated to the ambient air through the radiator. It is determined using equation (2), as function of the coolant mass flow rate and the coolant inlet and outlet temperatures in the radiator.

$$\dot{Q}_{radiator} = \dot{m}_{Radiator}(H_i - H_e) \tag{2}$$

Where, H_i and H_e are the enthalpies of the engine-coolant at the inlet and the outlet of the radiator respectively.

Referring to figure 1, the coolant flow rate ($\dot{m}_{Radiator}$) can be deduced from equation (3).

$$\dot{m}_{Engine} = \dot{m}_{Radiator} + \dot{m}_{CHU} + \dot{m}_{Recirculation} \tag{3}$$

Where $\dot{m}_{Engine}$ is the engine-coolant inlet mass flow rate, $\dot{m}_{CHU}$ the coolant flow rate serving to heat the cabin and $\dot{m}_{Recirculation}$ the coolant flow rate used in the recirculation loop namely during engine warm ups.

Figure 2 illustrates the coolant thermal power rejected from the radiator at each engine operating point on the engine map. This map was compiled from test bench measurements of a 1.2 liters turbocharged gasoline engine, using thermocouples at the inlet and outlet of the radiator, and a water flow meter at the outlet of the cylinder head. The used engine-coolant fluid during the experiment is a water and glycol mixture; however, it is assumed as pure water in the calculation. The measurements were performed in steady state at each engine operating point.

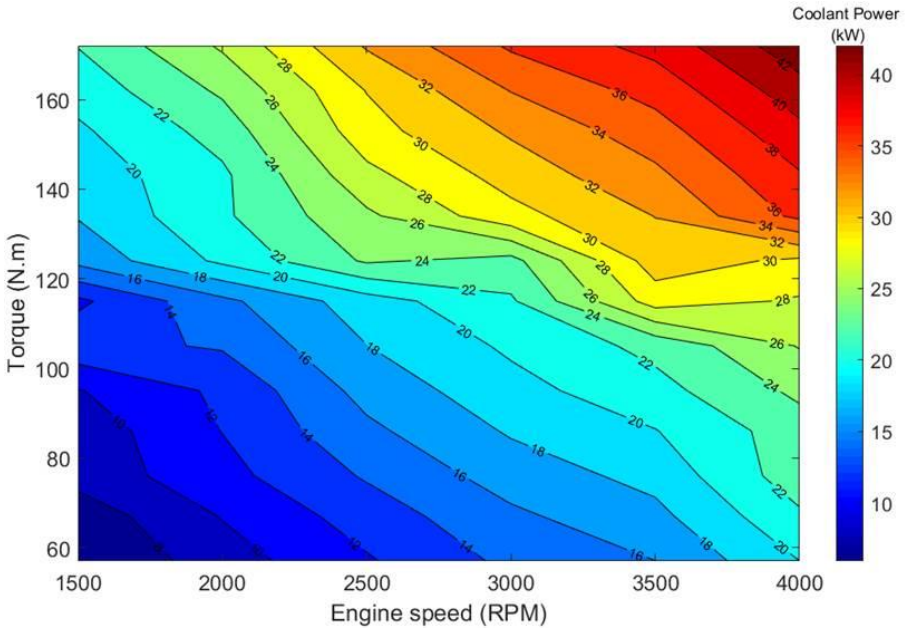

Fig. 2. Coolant thermal power rejected from the radiator.

2.3.2. Overall efficiency of the heat recovery system

This section presents the thermodynamic model of the ORC heat recovery system, and calculates the overall efficiency of heat conversion to mechanical work for a given engine-coolant temperature map. As shown in figure 1, the heat exchanger serves as the energy source for the ORC and consists of

three parts: heater, boiler and superheater, illustrated in the T-S diagram of figure 3. For simplicity, it will be referred to in this paper as heat exchanger (Hx).

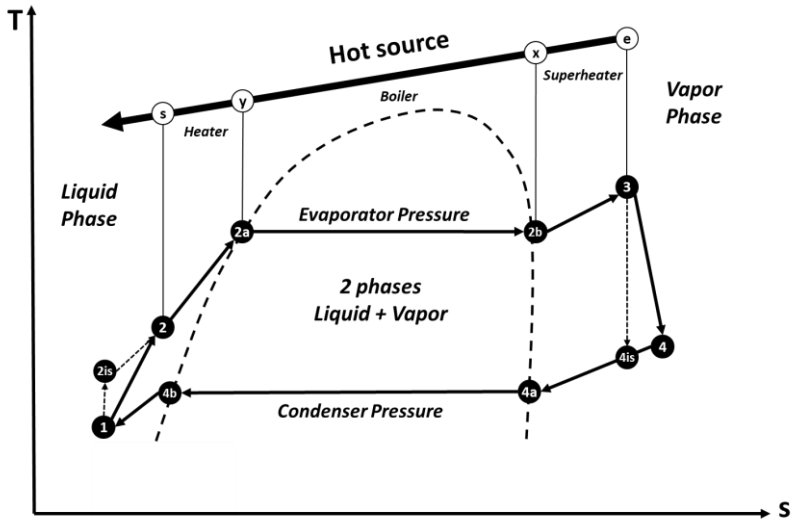

Fig. 3. T-s diagram for Rankine cycle recovering heat from an energy source.

In order to model the cycle, the pinch is defined as the minimum temperature difference in the heat exchanger, a positive value to ensure a heat exchange between engine-coolant and the working fluid (equation 4).

$$Pinch = T_y - T_{2a} \tag{4}$$

The overheating is defined as the difference between the temperature of the fluid at the outlet of the heat exchanger and the saturated vapor temperature of the fluid at the same pressure (equation 5). A zero or positive overheating is required to ensure vapor state at turbine inlet.

$$Overheating = T_3 - T_{2b} \tag{5}$$

The subcooling is defined as the difference between the temperature of the fluid at the outlet of the condenser and the saturated vapor temperature of the fluid at the same pressure (equation 6). A zero or positive subcooling is required to ensure liquid state at pump inlet.

$$Subcooling = T_{4b} - T_1 \tag{6}$$

Neglecting the internal irreversibility and pressure losses in the heat exchanger, condenser and piping, the work of the turbine and the pump, as well as the amount of heat exchanged in the heat exchanger and the condenser are calculated per unit mass by reference to figure 1, and using equations (7) to (10).

$$\frac{\dot{W}_{turbine}}{\dot{m}_{WF}} = h_3 - h_4 \tag{7}$$

$$\frac{\dot{W}_{Pump}}{\dot{m}_{WF}} = h_2 - h_1 \tag{8}$$

$$\frac{\dot{Q}_{Hx}}{\dot{m}_{WF}} = h_3 - h_2 \tag{9}$$

$$\frac{\dot{Q}_{condenser}}{\dot{m}_{WF}} = h_4 - h_1 \tag{10}$$

The Rankine cycle efficiency is the ratio of the net work produced and the amount of heat supplied to the heat exchanger by the engine-coolant (equation 11).

$$\eta_{Rankine\ Cycle} = \frac{\frac{\dot{W}_{turbine}}{\dot{m}_{WF}} - \frac{\dot{W}_{pump}}{\dot{m}_{WF}}}{\frac{\dot{Q}_{Hx}}{\dot{m}_{WF}}} = \frac{W_{net}}{Q_{Hx}} = \frac{(h_3 - h_4) - (h_2 - h_1)}{h_3 - h_2} \tag{11}$$

However, the maximal thermal capacity that can be evacuated through the radiator ($\dot{Q}_{radiator}$) is defined in equation (2), then the heat extraction efficiency at the coolant level can be defined in equation 12 as follow:

$$\eta_{Extraction} = \frac{H_e - H_s}{H_e - H_i} = \frac{Q_{Hx}}{Q_{radiator}} \tag{12}$$

Consequently, the overall efficiency defined as the ratio of the net work to the maximal heat capacity available in the coolant (equation 13) is the product of the Rankine cycle efficiency ($\eta_{Rankine\ Cycle}$) and the extraction efficiency ($\eta_{Extraction}$) (equation 14). Therefore, the overall efficiency optimization requires investigating both terms of the equation, as discussed in section 2.3.3.

$$\eta_{overall} = \frac{W_{net}}{Q_{Radiator}} = \frac{W_{net}}{Q_{Hx}} \times \frac{Q_{Hx}}{Q_{Radiator}} \tag{13}$$

$$\eta_{overall} = \eta_{Rankine\ Cycle} \times \eta_{Extraction} \tag{14}$$

2.3.3. Overall efficiency optimization

The optimization of the ORC overall efficiency requires the maximization of both the Rankine cycle efficiency ($\eta_{Rankine\ Cycle}$) and the heat extraction efficiency ($\eta_{Extraction}$) combined. Two parameters are identified to largely affect these efficiencies: the heat exchanger pressure (P_3) and the working fluid's highest temperature (T_3) (or the overheating (T_3-T_{2b})) [32]. In fact, the Rankine cycle efficiency increases with increasing the heat exchanger pressure or the overheating; however the extraction efficiency from the engine-coolant decreases drastically, which deteriorates the overall efficiency. Therefore, the Rankine cycle efficiency and the heat extraction efficiency calculations are made as function of these two parameters (P_3) and (T_3-T_{2b}), and the NSGA multi-objective genetic algorithm is used to determine the Pareto optimal overall efficiency solution [33]. It is noteworthy to mention that increasing the pressure in the heat exchanger presumes additional stringent requirements on the design, which results in cost and weight increase.

The calculation methodology is illustrated in figure 4. The Rankine cycle efficiency and the heat extraction efficiency calculations are performed first using the Refprop software [47] and a set of input parameters such as the water coolant inlet and outlet temperatures, the subcooling value and the pump and turbine efficiencies, as summarized in table 1. These parameters correspond to component specifications and to design constraints. The NSGA optimizations are performed with a minimum pinch value constraint of 5°C in order to limit the evaporator exchange surface [34-36]. Note that the pressure drop in the ORC system is neglected as it contributes to only 0.6% drop in the overall

efficiency. The negligible impact of the pressure drop on the efficiency is due to the advantage of using the R-1234yf working fluid, which circulates in the liquid-gas form in the system. For reference, typical pressure drop values in the condenser and the heat exchanger are 50 mbar and 75 mbar respectively.

Table 1. Input parameters based on components specifications and design constraints.

Parameter	Unit	Value	Remark
Maximum cycle pressure	MPa	3	Maximum allowed pressure to avoid operating the working fluid in its supercritical state, as the supercritical pressure of the R-1234yf is 3.2 MPa.
Condensing temperature	°C	35	Assumption for 20°C ambient temperature.
Subcooling	°C	2	To ensure a liquid phase at the pump inlet.
Coolant inlet temperature	°C	85-105°C	Given based on engine operating point.
Pump efficiency	%	65	From literature. Note that this used value corresponds to the efficiency of the pump and its electric drive machine combined.
Turbine efficiency	%	70	From literature.

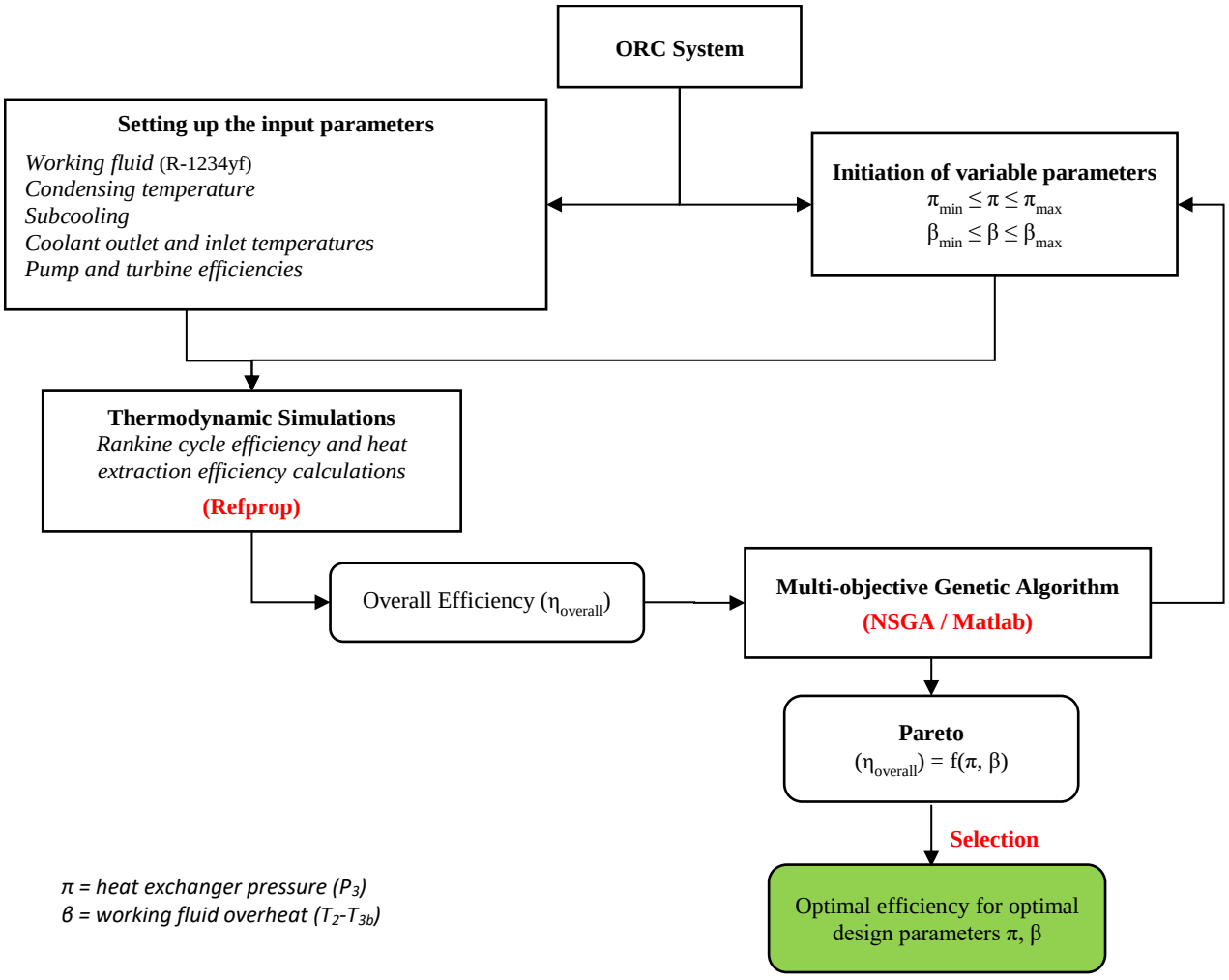

Fig. 4. Methodology for the determination of the maximum overall efficiency and the optimal pressure and overheating parameters as function of the water coolant temperature.

Figure 5 illustrates the resulting optimal overall efficiency solution, pinch and maximum cycle pressure for the two different engine-operating points 85°C (at high engine load) and 105°C (at low load). Results show that the max cycle pressure (respectively the pinch) varies from 22.4 bars to 30 bars (from 5°C to 13°C) for the 85°C and 105°C engine-coolant temperatures. The overall efficiency varies then from 6.6% to 7.8% respectively. Consequently, the resulting available mechanical power generated by the turbine is illustrated in figure 6 for each engine operating point.

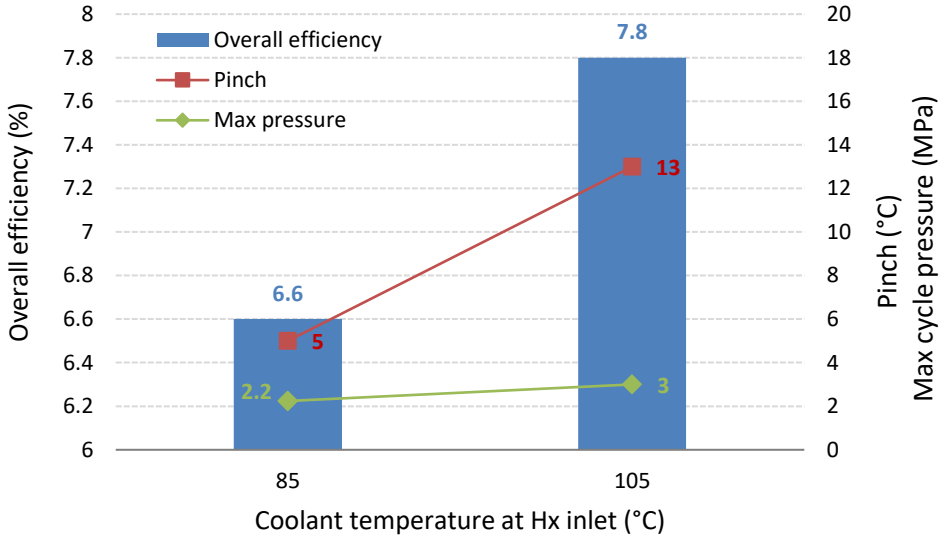

Fig. 5. Maximum overall efficiency and optimum pinch and cycle pressure for 85°C and 105°C engine-coolant temperatures.

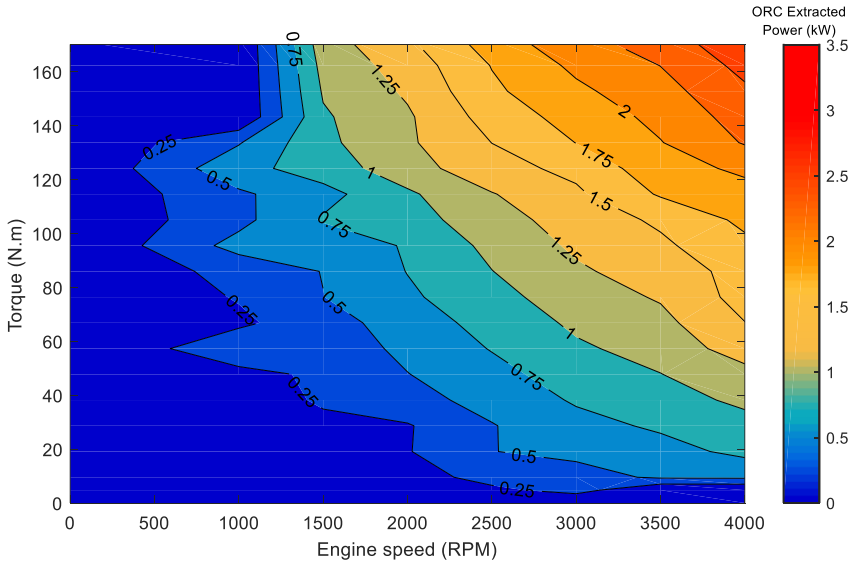

Fig. 6. Available mechanical power extracted from the ORC system at each engine operating point.

The overall efficiency presented in figure 5 and the resulting available mechanical power of figure 6 corresponds to the vehicle operation in moderate climates, with 20°C ambient temperature and 35°C condensing temperature. Figure 7 illustrates the overall efficiency variation taking into account colder and hotter climates and consequently cooler and hotter condensing temperature. For instance, results at 45°C condensing temperature show a drop of efficiency from 6.6% to 5% for the engine-coolant at 85°C and from 7.8% to 6.4% for the coolant at 105°C.

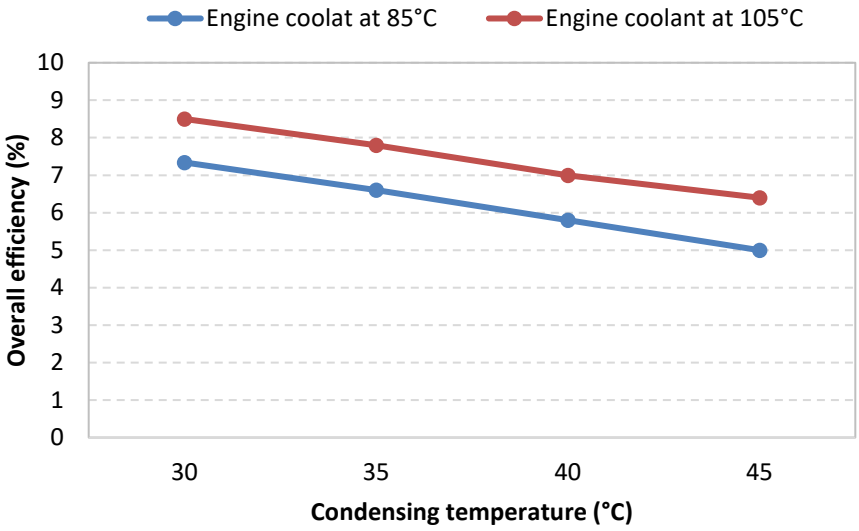

Fig. 7. Overall efficiency variation as function of the condensing temperature.

It is also interesting to inquire about the evacuated power from the condenser in order to ensure its proper sizing and implementation in the vehicle. Figure 8 illustrates the WLTC velocity profile and the evacuated power from the condenser for a condensing temperature of 35°C and coolant temperature of 85°C. The average evacuated power from the condenser is around 3.6 kW; consequently, implementing a small 10 kW ORC condenser similar to the AC condenser size is adequate. The evacuated power values exceeding 10 kW occur at high vehicle speed (above 80 km/h), and in that case the blowing air on the condenser resulting from the vehicle motion is sufficient to cool the working fluid. Note that the radiator fans in passenger vehicles are turned off at vehicle speed exceeding 70 km/h as the air blowing on the radiator is sufficient to cool the engine coolant. Therefore, a 10 kW condenser is appropriate in this case.

Figure 9 illustrates the evacuated power from the condenser at 45°C condensing temperature, which corresponds to extreme hot weather conditions. The observed average evacuated power is 4.9 kW, and power values exceeding 10 kW correspond to vehicle speeds above 60 km/h. In this case, a 15 kW condenser is required as a safety measure. Another safety measure is conceived in the design, switching off the ORC system under severe conditions or in case of failure. In this case, the engine-coolant is redirected into the main vehicle radiator as illustrated in figure 1 (blue lines).

It is also noteworthy to mention that the vehicle main radiator size can be reduced in the case of this study, and by this, allowing more space for integrating the ORC condenser, without affecting the drag coefficient of the vehicle.

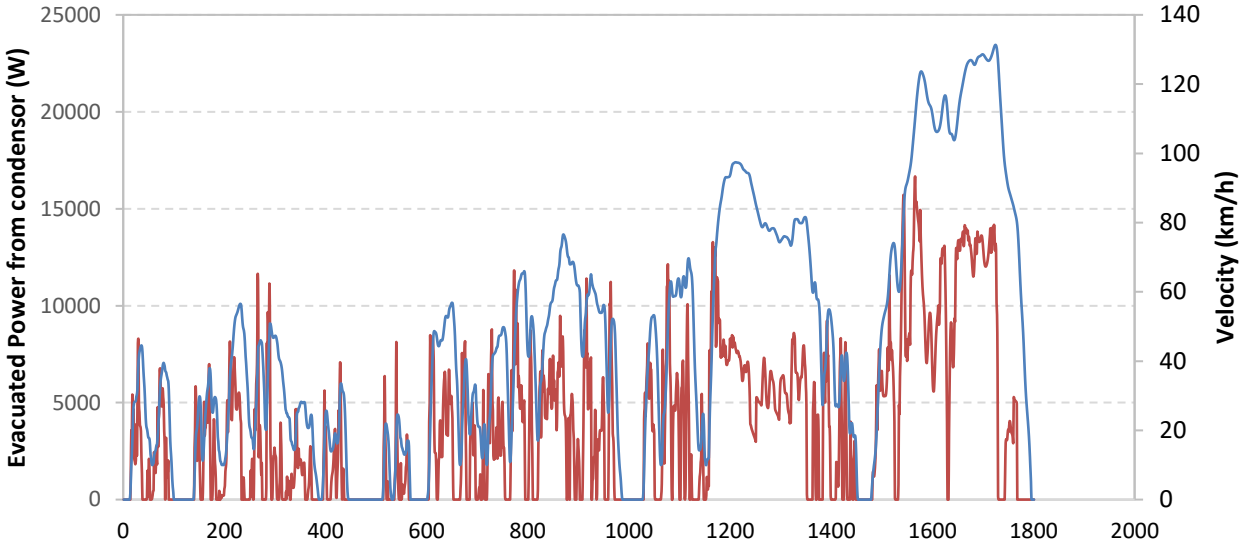

Fig. 8. Evacuated power from the condenser 35°C condensing temperature and 6.6% overall efficiency.

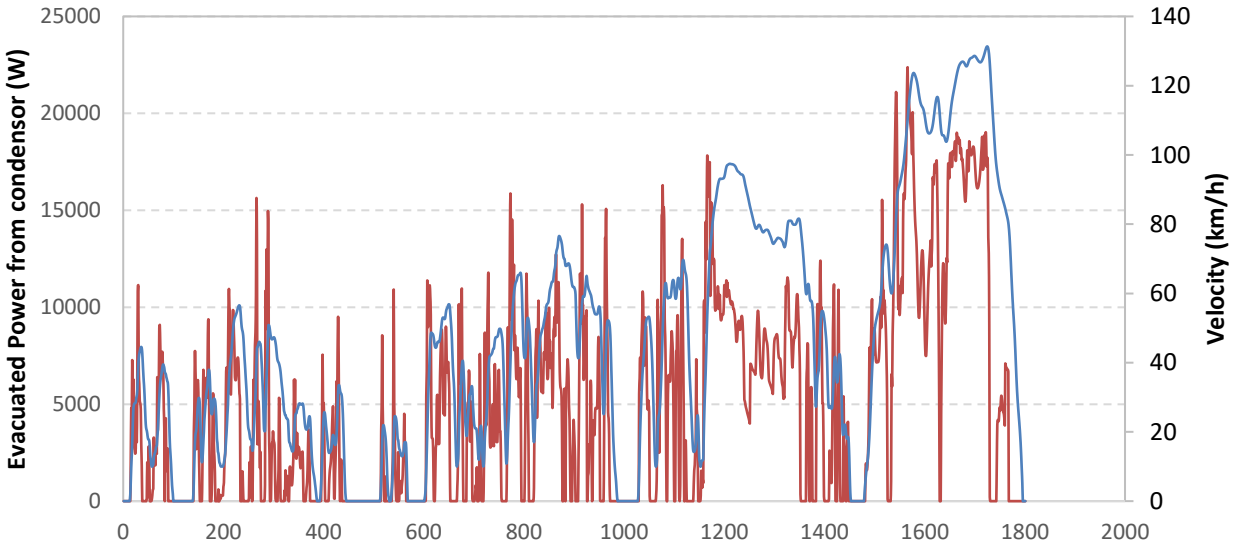

Fig. 9. Evacuated power from the condenser at 45°C condensing temperature and 5% overall efficiency.

3. Mild hybrid vehicle model

In order to evaluate the benefit of the ORC system described above in terms of fuel savings, a mild hybrid vehicle is considered, where the ORC system deployed recovers the engine-coolant energy, and the resulting mechanical power obtained from the turbine is converted into electrical power stored in the battery. A mild hybrid vehicle was chosen due to the rising interest of vehicle manufacturers in replacing the conventional powertrains with low-level electrified ones. This section presents the vehicle model and coupling setup of the powertrain and the studied ORC, as well as the modeling approach and vehicle control used to estimate the fuel consumption and assess the gain obtained from the ORC.

3.1. Powertrain setup and modeling approach

The powertrain architecture corresponds to a front-wheel drive parallel mild-hybrid configuration, combining a thermal conventional powertrain to an electric machine working in both modes: motor and generator, as illustrated in figure 10. The thermal powertrain consists of a 1.2 liters turbocharged engine, providing a maximum of 97 kW, and a 5-gear manual gearbox. The clutch model was disregarded for simplicity and the gear change is assumed instantaneously. The engine is modeled as a mechanical power source with a quasi-static efficiency map coupled to an inertia emulating the dynamic behavior of the engine rotating components. The engine map is illustrated in figure 11.

The electric machine consists of a belt driven starter-alternator with a 2.2:1 speed ratio. In addition to its conventional starter and alternator functions, this machine is enquired to recover braking and deceleration energy (generator mode), and to launch the engine and ensure torque assist during high load driving patterns (motor mode). Consequently, the size of the machine was optimized in order to minimize the fuel consumption on NEDC and WLTC drive cycles. The optimization routine was the dynamic programming in order to exclude the impact of the control strategy on the consumption and rather only identify the impact of the electric machine size on the consumption. Different size of starter-alternator where considered; however, since this optimization process falls out of the scope of this paper, only the results are highlighted in figure 12. The 10 kW starter-alternator was selected and modeled similarly to the engine, via an inertia and a quasi-static efficiency map for the electro-mechanical conversion in both motor and generator modes (figure 13). The power electronics module efficiency is included in the machine efficiency map.

A NiMH battery with a 1.1 kWh energy capacity is considered as a buffer and represented by a simple battery model of voltage source and internal resistance with a coulombic efficiency of 95% [37]. The vehicle chassis corresponds to a mass-production C-segment vehicle with a weight of 1474 kg. The ORC system illustrated in figure 1 is integrated in the vehicle model, and the energy recovered from the coolant is converted into electrical energy through a 70% efficiency electric generator, and stored in the battery. The components sizing of the ORC was carried out and a total weight of 15 kg is obtained.

The described powertrain configuration offers three possible forward driving modes and one neutral mode where the vehicle is at rest and the engine switched-off. In that case, only the auxiliaries' electric consumption is withdrawn from the battery, averaged at 294 W. The three driving modes are: (1) the conventional (pure) engine mode, (2) the motor assist mode where both the engine and the motor provide torque for traction, and (3) the brake recovery mode where the engine is switched-off and the vehicle kinetic energy is partially recovered by the alternator. Note that no clutch separates between the engine flywheel and the electric machine; therefore, part of the recovered brake energy is dissipated through the engine drag torque.

Each of the driving modes is decided by the vehicle control strategy depending on the driving conditions. Hybrid vehicle control strategies are classified in the literature under two main categories: rule-based strategies and optimization-based strategies [38, 39]. In the first category, the control consists of a set of rigid rules that decides the operating modes according to the driving pattern (load), the battery available energy and the driver power request. The rules are elaborated either through engineering intuition algorithms based on the components efficiency maximization [40, 41] or through fuzzy-logic control techniques [42]; consequently, the vehicle consumption is biased by the used control strategy. On the other hand, the optimized-based strategies consist of finding the optimal consumption based on prior knowledge of the upcoming patterns on the driving cycle [43]. Among the techniques frequently used is the dynamic programming (DP) which ensures the optimal fuel saving over the scheduled driving cycle. Consequently, DP excludes the impact of the energy management strategy on the vehicle consumption.

Since the purpose of this study is to evaluate the fuel savings potential of the considered mild hybrid vehicle with an embedded ORC system recovering the engine-coolant energy, the DP control strategy is used in order to eliminate the impact of the control strategy on the consumption and identify only the benefit of the ORC system.

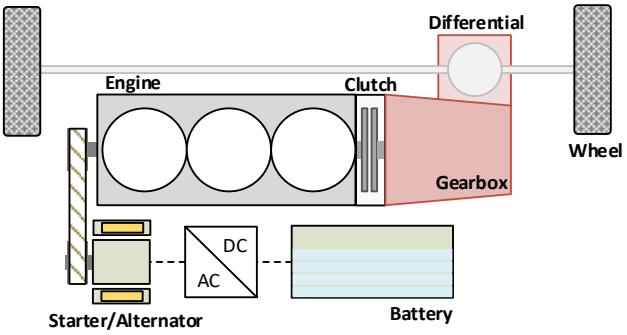

Fig. 10. The investigated front-wheel drive parallel mild hybrid powertrain architecture.

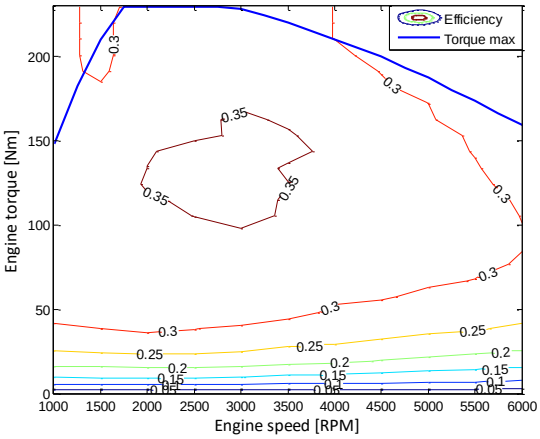

Fig. 11. Engine efficiency map.

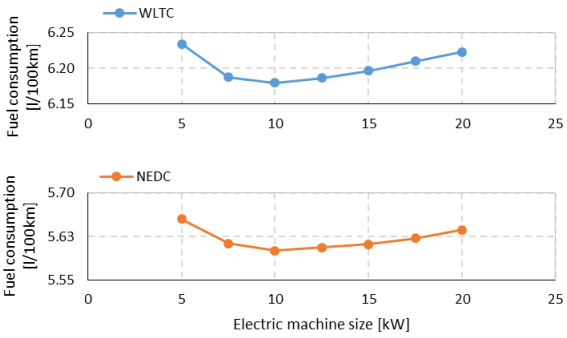

Fig. 12. Optimization results of the starter-alternator power sizing on NEDC and WLTC.

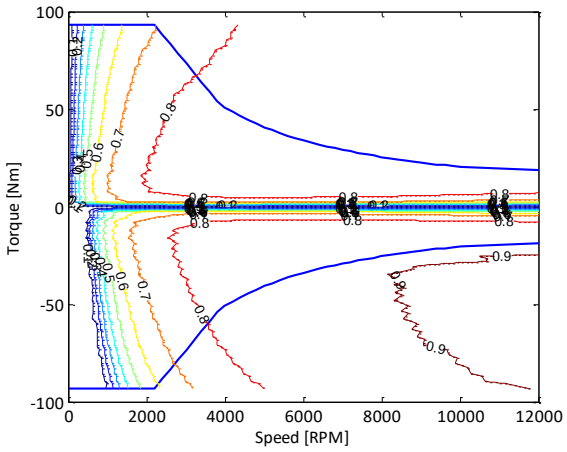

Fig. 13. Starter-alternator efficiency map.

3.2. Powertrain quasi-static model

The powertrain model presented in this section is elaborated to assess the energy flow within the components and determine the energy consumption on the driving cycles taking into account the contribution of the investigated ORC system. Hence, a feed-backward simulation of the chassis and the powertrain components is considered, emulating the inverse energy flow from the "wheel" (vehicle driving load) to the "tank" (the battery and the fuel tank), as illustrated in figure 14. Only longitudinal dynamics of the chassis are considered and on flat roads.

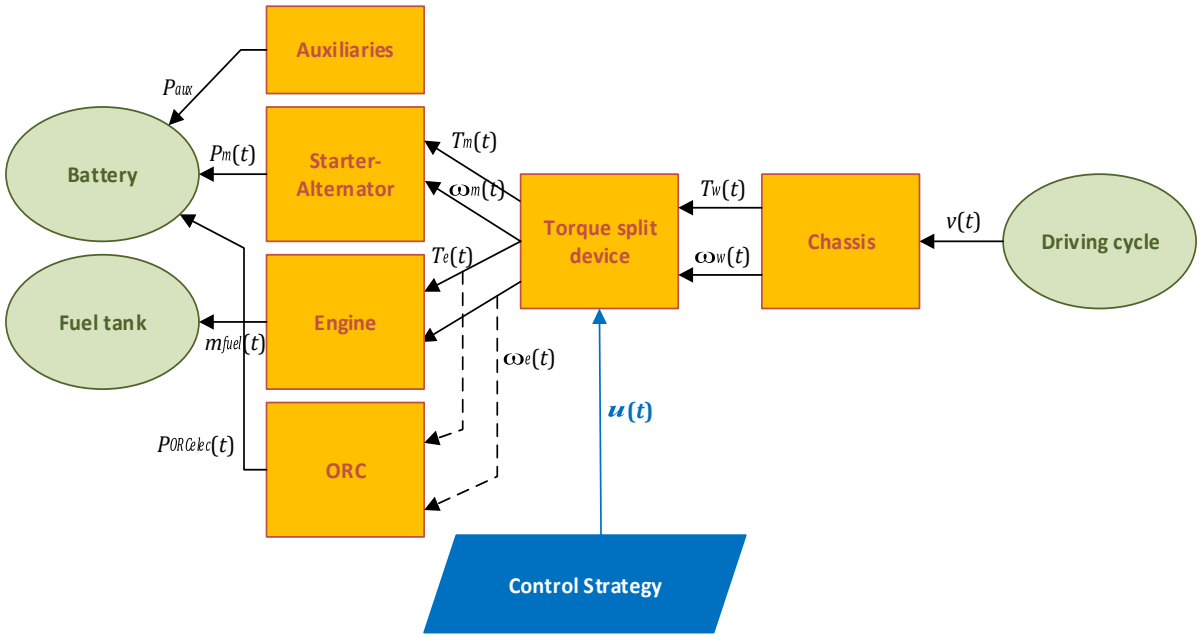

Fig. 14. Vehicle backward model.

Chassis model - It intends to determine the force required to overcome the load applied to the vehicle at instant *t*. It consists of the aerodynamic drag force, rolling resistance and the inertia force of the vehicle. This force in addition to the known vehicle speed at *t* result in a torque demand at the wheels (T_w) and a wheel speed (ω_w) (equations 15 and 16).

$$T_w(t) = \left(\frac{1}{2}\rho S C_x v(t)^2 + M g f_r v(t) + M\frac{dv(t)}{dt}\right) \times R_w \tag{15}$$

$$\omega_w(t) = \frac{v(t)}{R_w} \tag{16}$$

Torque split devise - The torque demand (T_w) has to be provided either by the engine, or split between the engine (T_e) and the electric machine (T_m). That's during traction mode; however, during braking and deceleration, the electric machine recovers the vehicle energy while the engine is kept off $(T_e = 0)$. Consequently, a torque split ratio $u(t)$ is introduced in order to express T_e and T_m as function of T_w under the three highlighted driving modes (equations 17 to 20). The value of $u(t)$ ranges between 0 and 1, where a value of 0 corresponds to the (pure) engine drive mode, and 1 to the electric mode. However, since the investigated vehicle is a mild hybrid, the electric machine is not sized to ensure electric drive mode, thus the torque split ratio is constrained to be lower than 1. Therefore, the upper limit of $u(t)$ is constrained by forcing the engine speed to exceed 1000 RPM in order to ensure its capability in providing the sufficient requested traction torque. Values of $u(t)$ between 0 and 1 indicate that both the engine and the motor provide torque for traction, referred to as the boosting mode. Note that for brake recovery mode, $u(t)$ is assigned the value -1, and T_e is nulled.

Control strategy – Its role is to determine at each instant *t* the torque split ratio $u(t)$ [44]. This function is realized through the optimal-based DP strategy, explained in the next section. In brief, The DP control determines the optimal set of torque split ratio $u(t)$ at each time instant *t* and consequently guarantees the optimal consumption at the end of the driving cycle.

$$T_{crank}(t) = \begin{cases} \dfrac{T_w(t)}{k_i \times \eta_{trans}} + T_{e_{drag}}(t) + T_{m_{drag}}(t), & \dfrac{dv}{dt} \geq 0 \\ \dfrac{T_w(t) \times \eta_{trans}}{k_i} + T_{e_{drag}}(t) + T_{m_{drag}}(t), & \dfrac{dv}{dt} < 0 \end{cases} \quad (17)$$

$$T_{total\ load}(t) = T_{crank}(t) + T_{e_{drag}}(t) + T_{m_{drag}}(t) \quad (18)$$

$$T_e(t) = \big(1 - u(t)\big) \times T_{total\ load}(t) \quad (19)$$

$$T_m(t) = \frac{u(t) \times T_{total\ load}(t)}{k_{belt}} \quad (20)$$

With T_{crank}: torque drive demand at the crankshaft (deduced from the load at the wheel through backward calculation)

$T_{e_{drag}}$: engine drag torque (including inertia)

$T_{m_{drag}}$: electric machine drag torque (including inertia)

$T_{total\ load}$: total load torque requested (including the engine and machine drag torques)

η_{trans}: transmission efficiency (gearbox and final drive combined)

k_i: transmission ratio (gearbox and final drive combined)

k_{belt}: ratio between the engine and the starter-alternator (2.2:1)

Engine, ORC and battery models - Once $u(t)$ is determined, the engine torque and speed are evaluated from equations 19 and 21, and the fuel mass flow rate $\dot{m}(t)$ is computed by linear interpolation using the engine map of figure 11. Similarly, the ORC mechanical power $P_{ORC_{mech}}(t)$ recovered from the engine-coolant is determined using the methodology presented in section 2 as function of the engine-coolant temperature. The latter is determined by linear interpolation for the corresponding engine torque and speed from the engine-coolant map. This mechanical power is converted into electrical power and stored in the battery for a later use by the electric machine. Consequently, the battery power (P_{batt}) exchanged with the different powertrain components is the resultant combination of the electric machine power (P_m), the auxiliaries power (P_{aux}) and the ORC electrical generated power ($P_{ORC_{elec}}$) as expressed in (equation 23). The battery current $I(t)$ and state-of-charge $SOC(t)$ are computed using equations 24 and 25 respectively. The open circuit voltage $V_{oc}(t)$ and battery internal resistance $R_{int}(t)$ are illustrated in figure 15, and the battery maximum capacity (C_{max}) is 5.5 Ah.

$$\omega_e(t) = \begin{cases} \dfrac{k_i}{R_w} \times v(t), & clutch\ engaged \\ 0, & clutch\ disengaged \end{cases} \quad (21)$$

$$\omega_m(t) = k_{belt} \times \omega_e(t) \quad (22)$$

$$P_{batt}(t) = P_m(t) + P_{aux}(t) - P_{ORC_{elec}}(t) \quad (23)$$

$$I(t) = \frac{V_{oc}\big(SOC(t)\big) - \sqrt{V_{oc}^2\big(SOC(t)\big) - 4\,P_{batt}(t)\,R_{int}\big(SOC(t)\big)}}{2\,R_{int}\big(SOC(t)\big)} \quad (24)$$

$$SOC(t) = \frac{C_{ini} + \int_{t_0}^{t} I(t)\,dt}{C_{max}} \quad (25)$$

In order to ensure the feasibility of the obtained results, some constraints are added to the model to eliminate the unrealistic components operating points. The maximum and minimum torque and speed constraints for the engine and the electric motor are provided in figures 11 and 13 respectively. The power constraints of these two components can be deduced from the resulting torque and speed

product. Therefore, the power constraints depend on the value of the engine or motor running speed. Moreover, the battery life is preserved by limiting the current between -85A and 100A, and narrowing the SOC range to 40% of the battery capacity, placed in symmetry around 60% ($SOC \in [0.4, 0.8]$).

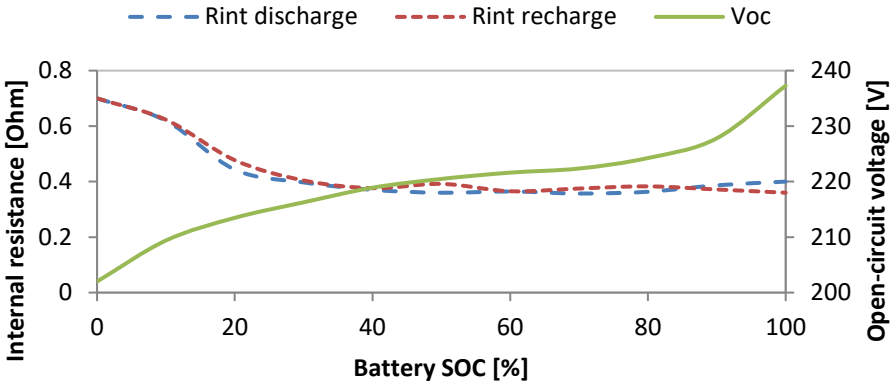

Fig. 15. Battery open-circuit voltage and internal resistance.

3.3. Dynamic programming control strategy

DP is a mathematical technique used to determine the global optimal of a cost function J which corresponds to the total mass of fuel to be consumed over the desired finite time horizon driving cycle (equation 26) [43, 45].

$$J = \int_{t=0}^{N-1} \dot{m}_{fuel}\left(SOC(t), v(t), a(t), i_g(t), u(t)\right) dt \tag{26}$$

The fuel mass flow rate $\dot{m}(t)$ corresponds to the cost-to-go matrix in which the optimal costs to move from state $x(t)$ to the next state $x(t+1)$ by applying the control variable $u(t)$ are saved. The battery $SOC(t)$, the vehicle velocity $v(t)$, the acceleration $a(t)$ and the gear number $i_g(t)$ constitutes the state variables of the studied vehicle model, and the torque split ratio $u(t)$ its control variable. Since the scheduled driving cycle is assumed known beforehand, the velocity, acceleration and gear number are identified from the driving cycle profile at each time step, and consequently, the remaining state variable of the model is the battery SOC. Therefore, the optimization problem turns to minimize the cost function of equation 27, by computing backward in time from the final desired SOC to the initial SOC the optimal cost-to-go function $\dot{m}_{fuel}\big(SOC(k), u(k)\big)$ in the discretized state time space of SOC, with k the discretized time instance. Hence, the DP problem can be discretized and formulated as presented in equations 28 to 32.

Note that only hot engine operations are considered, therefore, no additional consumption is accounted for the engine warm-ups. Moreover, the engine start, clutch actuation and gear shifting are assumed instantaneous, and thus the corresponding energy losses and additional fuel consumption are disregarded.

$$L = min\left\{\sum_{k=0}^{N-1} \dot{m}_{fuel}\big(SOC(k), u(k)\big) \times dt_s\right\} \tag{27}$$

with state variable equation:

$$SOC(k+1) = f\big(SOC(k), u(k)\big) + SOC(0) \tag{28}$$

initial SOC: $$SOC(0) = 0.6 \quad (29)$$

final SOC: $$SOC(N) = 0.6 \quad (30)$$

discrete step time: $$dt_s = 1 \quad (31)$$

number of time instances: $$N = \frac{n}{dt_s} + 1 \quad (32)$$ (with *n* the time length of the driving cycle)

The optimization problem consists then in taking the appropriate decisions of torque split ratio $u(k)$ at each time instance k in order to minimize the total fuel consumed (cost function J) over the scheduled driving cycle. The advantage of DP control consists in the decision-making trade-off made between the desire for low present consumption and the undesirable high future consumption. In fact, each torque split ratio $u(k)$ cannot be decided separately from the upcoming trip energy consumption. Consequently, the outcome of the DP algorithm applied to this optimization problem is the optimal torque split strategy $U_{opt} = \{u_0, \dots, u_{n-1}\}_{opt}$ for the scheduled driving cycle. It specifies the optimal torque split ratio $u(k)$ at each time instance k and the resulting optimal SOC trajectory. The initial and final SOC are imposed to be the same in order to evaluate only the fuel consumption at the end of the trip.

Note that the resulting optimal control variable $u(k)$ must not violate the components constraints in terms of torque, speed, power, current and SOC, defined in section 3.2 (equations 33 to 38), in order to ensure the proper functioning of the components within the normal operating range.

Battery power: $$P_{b_{min}} \leq P_b(k) \leq P_{b_{max}} \quad (33)$$

Battery SOC: $$SOC_{min} \leq SOC(k) \leq SOC_{max} \quad (34)$$

Motor torque: $$T_{m_{min}}(\omega_m(k)) \leq T_m(k) \leq T_{m_{max}}(\omega_m(k)) \quad (35)$$

Motor speed: $$0 \leq \omega_m(k) \leq \omega_{m_{max}}(k) \quad (36)$$

Engine torque: $$T_{e_{min}}(\omega_m(k)) \leq T_e(k) \leq T_{e_{max}}(\omega_m(k)) \quad (37)$$

Engine speed: $$0 \leq \omega_g(k) \leq \omega_{g_{max}}(k) \quad (38)$$

4. Results

The suggested ORC system is evaluated in this section by comparing the fuel consumption of two different powertrain configurations for the same-modeled mild hybrid vehicle. The first powertrain model does not include the ORC system and serves as the reference (referred to in this section as "reference powertrain"). The second model includes the ORC in the powertrain as described in section 3.1 (referred to as "ORC powertrain"). Note that the simulations are conducted on NEDC and WLTC, with a zero use of electric energy from the battery at the end of the cycle $(SOC_{initial} = SOC_{final} = 60\%)$, in order to evaluate the fuel consumption only. Moreover, the results reflects the impact of the suggested ORC system in moderate climate conditions as presented in table 1. This is to illustrate the average impact of the studied ORC system on the vehicle consumption.

Figures 16 and 17 compares the different driving modes share distribution of the two configurations on NEDC and WLTC. Four different driving modes are observed: (pure) engine mode, boosting mode (engine and motor torque are combined), brake energy recovery (BER) mode and rest mode where the vehicle and the engine are stopped.

Results show that both powertrains spend 40% and 33% of the time on NEDC and WLTC respectively in either braking or vehicle rest modes; therefore, the remaining 60% and 67% are spent in traction modes: engine and boosting modes. The main advantage of the ORC powertrain on both

cycles consists of managing efficiently the traction modes, by relying further on the electric boosting mode, namely during acceleration phases. In fact, as illustrated in the figures, the (pure) engine mode time was reduced by 5.8% and 7.1% on NEDC and WLTC respectively as compared to the reference powertrain, and the electric boost mode share increased by 25% and 37%. This has consequently led to reduce the average engine power over both driving cycles, and on the counterpart, increase the average power of the electric motor, as illustrated in figure 18. This has been possible with the ORC powertrain due to the additional electric energy generated by the ORC from the engine-coolant waste heat recovery.

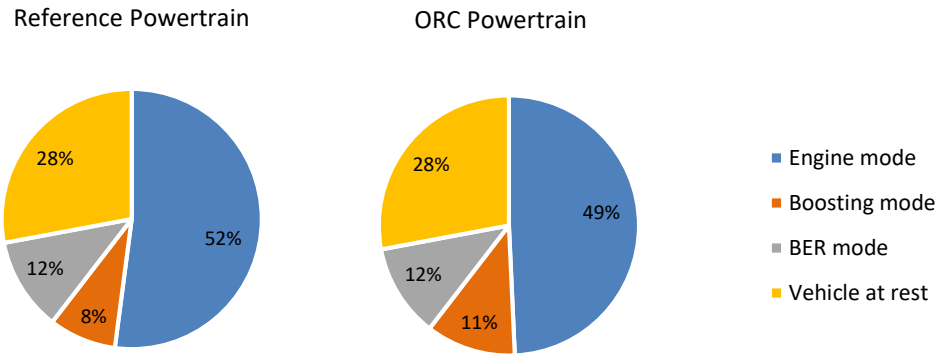

Fig. 16. Drive mode time distribution on NEDC.

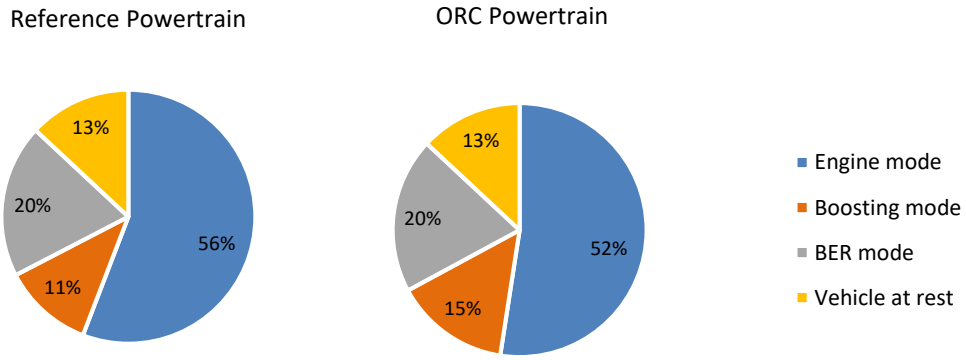

Fig. 17. Drive mode time distribution on WLTC.

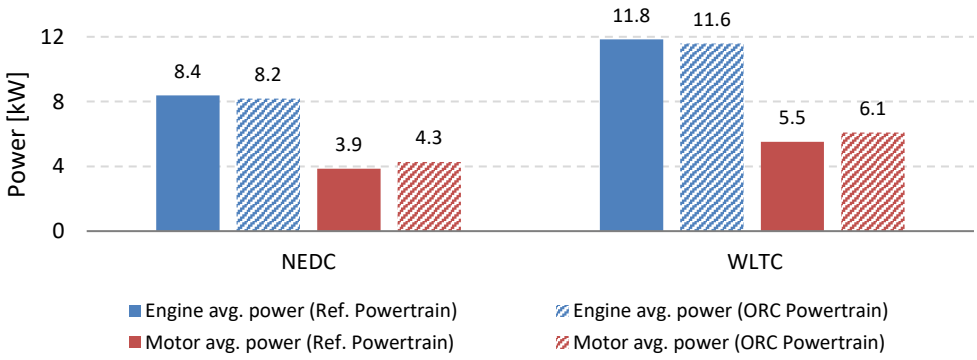

Fig. 18. Average power comparison of the engine and the motor on NEDC and WLTC for the simulated powertrains.

Figures 19 and 20 compare the engine and powertrain efficiencies (computed using equations 39 and 40), as well as the fuel consumption of both powertrains on the NEDC and the WLTC. The ORC powertrain shows an increase in the engine and powertrain efficiency compared to the reference powertrain. This consequently results in a decrease in the fuel consumption between 2% and 2.4% on the NEDC and the WLTC respectively. These results are in line with the fuel savings results presented in [50] on a hybrid vehicle, where the author demonstrated that the ORC recovery from engine-coolant improves the fuel efficiency between 1.7% and 2.8%.

Although savings are not large, they are estimated to be comparable to the vehicle auxiliaries' consumption, excluding the air conditioning.

$$\eta_{engine} = \frac{\int_{t_0}^{t_n} T_e(t) \times \omega_e(t)\, dt + \int_{t_0}^{t_n} P_{ORC_{mech}}(t)\, dt}{\int_{t_0}^{t_n} \dot{m}_{fuel}(t) \times H_v\, dt} \tag{39}$$

$$\eta_{powertrain} = \frac{\int_{t_0}^{t_n} P_{load}(t)\, dt}{\int_{t_0}^{t_n} \dot{m}_{fuel}(t) \times H_v\, dt + \int_{t_0}^{t_n} P_{batt_{BER}}(t)\, dt} \tag{40}$$

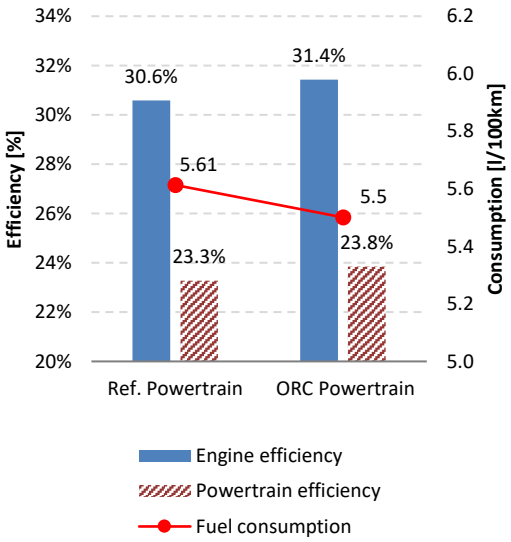

Fig. 19. Fuel consumption, engine and powertrain efficiencies on NEDC.

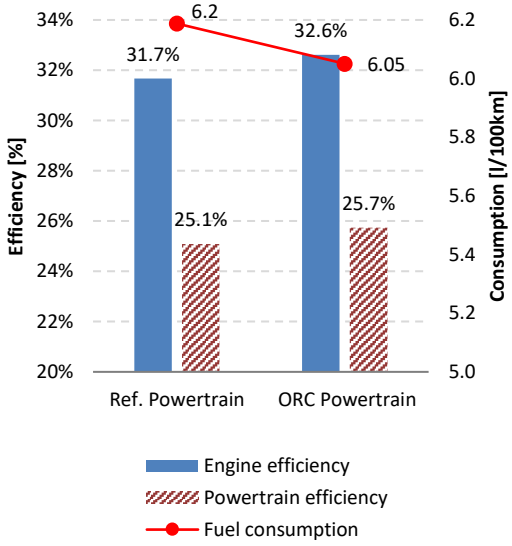

Fig. 20. Fuel consumption, engine and powertrain efficiencies on WLTC.

It is noteworthy to mention that several systems combination of waste heat recovery from engine-coolant and exhaust-gas heat recovery system can be considered to improve further the overall efficiency. For instance, an overall waste heat recovery up to 12.5% would improve the fuel savings up to 3.5% and 3.8% on the NEDC and the WLTC respectively. However, this will come at the expense of adding complexity and cost to the system in addition to vehicle integration challenges, likewise the existing ORC exhaust-gas waste recovery systems presented in the literature.

5. Summary and conclusions

This paper presented the assessment of an organic Rankine cycle on a mild hybrid vehicle, in order to explore the fuel savings potential from engine-coolant waste heat recovery. The coolant temperature is regulated to 85°C at high engine load and to 105°C at low load under any operating conditions, which helps maximizing the system overall efficiency at these two specific temperatures, unlike the case for waste heat recovery from exhaust gas. The recovered energy through this ORC

system is then converted into electricity and stored in the battery. The R-1234yf working fluid was used due to its isentropic properties, avoiding any diphasic expansion in the used expansion turbine.

The study proposed a methodology for optimizing the overall efficiency of the ORC, by presenting first the thermodynamic model of the cycle and then by applying the NSGA multi-objective genetic algorithm for optimizing the overall efficiency as function of two control parameters of the cycle: the maximum pressure cycle and the overheating. In addition, a detailed mild hybrid powertrain model is presented with an optimized start-alternator power size, and an optimal-based energy management strategy is proposed and detailed, using the dynamic programming optimization routine.

A reference mild hybrid powertrain and a mild hybrid powertrain including the ORC system were compared. Results showed that the ORC powertrain presented an engine and powertrain efficiency improvements, as well as consumption savings between 2% and 3% on the NEDC and the WLTC driving cycles, as compared to the reference powertrain. These savings were reflected by the share increase of the electric boosting mode over the two cycles, which resulted from the additional electric energy recovered from the engine-coolant through the ORC system over the trip. Although the observed energy savings are not large, they are on the order of the energy needed to power the vehicle auxiliaries.

Note that the calculations were made with some simplifying assumptions, such as considering table-based engine and motor maps, which do not capture components dynamics, and neglecting the power losses during vehicle gearshift, and the flow losses in the ORC system, as their impacts on the consumption were estimated negligible. As a result, the actual benefits of the considered system might be slightly lower.

References

[1] Arnaud L., Ludovic G., Mouad D., Hamid Z., Vincent L., Comparison and Impact of Waste Heat Recovery Technologies on Passenger Car Fuel Consumption in a Normalized Driving Cycle. Energies 2014, 7, 5273-5290; doi:10.3390/en7085273.

[2] Khalifa H. E., Waste heat recovery from adiabatic diesel engines by exhaust-driven Brayton cycles. DOE/NASA/0304-1, NASA CR-168257, December 1983.

[3] Amicabile S., Lee J., Kum D., A comprehensive design methodology of organic Rankine cycles for the waste heat recovery of automotive heavy-duty diesel engines. Applied Thermal Engineering, 2015.

[4] Ringler J., Seifert M., Guyotot V., Hübner W., Rankine Cycle for Waste Heat Recovery of IC Engines. *SAE Int. J. Engines* 2(1):67-76, 2009, https://doi.org/10.4271/2009-01-0174.

[5] Domingues A., Santos H., Costaa M., Analysis of vehicle exhaust waste heat recovery potential using a Rankine cycle. Energy, 2013.

[6] Saxena S., Ahmed M., Automobile Exhaust Gas Heat Energy Recovery Using Stirling Engine: Thermodynamic Model. SAE Technical Paper 2017-26-0029, 2017.

[7] Aladayleh W., Alahmer A., Recovery of Exhaust Waste Heat for ICE Using the Beta Type Stirling Engine. Journal of Energy, 2015

[8] Sahoo D., Kotrba A., Steiner T., Swift G., Waste Heat Recovery for Light-Duty Truck Application Using ThermoAcoustic Converter Technology. SAE Int. J. Engines 10(2):196-202, 2017, https://doi.org/10.4271/2017-01-0153.

[9] Fritzsche J., Drückhammer J., Käppner C., Hassel E., Steiner T., Thermoacoustics as an Alternative Technology for Waste Heat Recovery in Automotive and (Heavy) Duty Applications. 24th Aachen Colloquium Automobile and Engine Technology 2015.

[10] Stobart R., Wijewardane A., Allen C., The Potential for Thermo-Electric Devices in Passenger Vehicle Applications. SAE Technical Paper 2010-01-0833, 2010.
[11] Orr B., Akbarzadeh A., Mochizuki M., Singh R., A review of car waste heat recovery systems utilizing thermoelectric generators and heat pipes. Applied Thermal Engineering, 2015.
[12] Hussain Q., Brigham D., Maranville C., Thermoelectric Exhaust Heat Recovery for Hybrid Vehicles. *SAE Int. J. Engines* 2(1):1132-1142, 2009, https://doi.org/10.4271/2009-01-1327.
[13] Lua Y., Roskillya A. P., Smallbonea A., Yub X., Wanga Y., Design and parametric study of an Organic Rankine cycle using a scroll expander for engine waste heat recovery. The 8th International Conference on Applied Energy, Energy Procedia, 2017.
[14] E. F. Doyle, L. DiNanno, S. K : "Installation of a Diesel-Organic Rankine Compound Engine in a class 8 Truck for a Single-Vehicle Test", Society of Automotive Engineers, 790646, 1979.
[15]Espinosa N, Tilman L, Lemort V, Quoilin S, Lombard B "Rankine cycle for waste heat recovery on commercial trucks: approach, constraints and modeling", Volvo Powertrain France, University of Liège
[16] Dumand C, Bou Nader W, Coma G, Smague P, "Enjeux et évaluation de solutions de récupération d'énergie à l'échappement : une analyse du Groupement Scientifique Moteur, regroupant PSA, Renault et IFPEN" Pôle Mov'eo, Décembre 2014
[17] Ringler, J., Seifert, M., Guyotot, V., and Hübner, W., "Rankine Cycle for Waste Heat Recovery of IC Engines," SAE Int. J. Engines 2(1):67-76, 2009, doi:10.4271/2009-01-0174.
[19] Teng, H., Klaver, J., Park, T., Hunter, G. et al., "A Rankine Cycle System for Recovering Waste Heat from HD Diesel Engines - WHR System Development," SAE Technical Paper 2011-01-0311, 2011, doi:10.4271/2011-01-0311
[20] Park, T., Teng, H., Hunter, G., van der Velde, B. et al., "A Rankine Cycle System for Recovering Waste Heat from HD Diesel Engines - Experimental Results," SAE Technical Paper 2011-01-1337, 2011, doi:10.4271/2011-01-1337
[21] Furukaa T, Nakamura M, Machida K, Shimokawa K, "A study of the Rankine Cycle Generating System for Heavy Duty HV Trucks." Hino Motors, Ltd. SAE Technical Paper 2014-01-0678, 2014, doi:10.4271/2014-01-0678
[22] Endo T, Kawarjiri S, Kojima Y, Takahashi K, Baba T, Ibaraki S, Takahashi T, Shinohara M "Study on Maximizing Exergy in Automotive Engines." SAE Technical Paper 2007-01-0257
[23] Ibaraki, S.; Endo, T.; Kojima, Y.; Takahashi, K.; Baba, T. & Kawajiri, S: "Study of efficiency onboard waste heat recovery system using Rankine cycle", Review of Automotive Engineers, 28, 307-313, 2007.
[24] Freymann R, Ringler J, Seifert M, Horst T, "The second generation Turbosteamer". MTZ Worlidwide 2012;73:18-23
[25] Freymann, R.; Strobl, W. & Obieglo, A.: "The Turbosteamer: a system introducing the principle of cogeneration in automotive applications", MTZ, 69, 20-27, 2008.
[26] Leduc P, Smague P, « Rankine System for Heat Recovery: an Interesting Way to Reduce Fuel Consumption » SIA 2013
[27] Smague P, Leduc P « Integrated Waste Heat Recovery System with Rankine Cycle » 22nd Aachen Colloquium Automobile and Engine Technology 2013
[28] Samaneh Daviran, Alibakhsh Kasaeian, Soudabeh Golzari, Omid Mahian, Shahin Nasirivatan and Somchai Wongwises, "A comparative study on the performance of HFO-1234yf and HFC-134a as an alternative in automotive air conditioning systems", Applied Thermal Engineering, January 2017
[29] T.C. Hung, "Waste heat recovery of organic Rankine cycle using dry fluids", Energy Conversion & Management 42 (2001) 539–553.
[30] Cha W, Kim K, Choi K, et al. « Optimum Working Fluid Selection for Automotive Cogeneration System". Tc 2010;374(240.7):132.2.
[31] V. Maizza, A. Maizza, "Unconventional working fluids in organic Rankine-cycles for waste energy recovery systems", Applied Thermal Engineering 21 (3) (2001) 381–390.

[32] Samer Maalouf, “Study and design of a thermodynamic system generating mechanical work from a hot source at 120°C”, thesis work, Ecole des Mines de Paris, 2013.
[33] Deb K, Pratap A, Agarwal S et al. A fast and elitist multiobjective Genetic Algorithm: NSGA-II. In: *IEEE Transactions on evolutionary computation*, Vol. 6, No. 2, APRIL 2002.
[34] Sarah Van Erdeweghe, Johan Van Bael, Ben Laenen and William D’haeseleer, “Influence of the pinch-point-temperature difference on the performance of the Preheat-parallel configuration for a low-temeprature geothermally-fed CHP”, Energy Procedia, September 2017
[35] Mohammed Khennich and Nocilas Galanis, “Optimal design of ORC systems with a Low-Temperature Heat Source”, Entropy, 2012.
[36] You-Rong Li, Jian-Ning Wang, Mei-Tang Du, Shuang-Ying Wu, Chao Liu and Jinliang Xu, “Effect of pinch point temperature difference on cost-effective performance of organic Rankine cycle”, International Journal of Energy Research, September 2013
[37] Liu W. Energy storage system modeling and control. In: Introduction to hybrid vehicle system modeling and control. John Wiley & Sons, 2013, pp. 131-197.
[38] Wirasingha, S.G.; Emadi, A., "Classification and Review of Control Strategies for Plug-In Hybrid Electric Vehicles," Vehicular Technology, IEEE Transactions on , vol.60, no.1, pp.111,122, Jan. 2011.
[39] Salmasi, F.R., "Control Strategies for Hybrid Electric Vehicles: Evolution, Classification, Comparison, and Future Trends," Vehicular Technology, IEEE Transactions on , vol.56, no.5, pp.2393,2404, Sept. 2007.
[40] Branimir Škugor, Joško Deur, Mihael Cipek, and Danijel Pavković, “Design of a power-split hybrid electric vehicle control system utilizing a rule-based controller and an equivalent consumption minimization strategy”. Proceedings of the Institution of Mechanical Engineers, Part D: Journal of Automobile Engineering May 2014 228: 631-648, first published on January 27, 2014
[41] Mansour C and Clodic D. Dynamic modeling of the electro-mechanical configuration of the Toyota Hybrid System series/parallel powertrain. International Journal of Automotive Technology 2011; 13, 143-166.
[42] Mohsen Derakhshan and Kourosh Heidari Shirazi, “Optimized fuzzy controller for a power–torque distribution in a hybrid vehicle with a parallel configuration” Proceedings of the Institution of Mechanical Engineers, Part D: Journal of Automobile Engineering December 2014 228: 1654-1674, first published on August 6, 2014.
[43] Mansour C and Clodic D. Optimized energy management control for the Toyota Hybrid System using Dynamic Programming on a predicted route with short computation time. International Journal of Automotive Technology 2012; 13, 309-324.
[44] Sciarretta A and Guzzella L. Supervisory control algorithms. In: Vehicle Propulsion Systems: Introduction to Modeling and Optimization. Springer, 2007, pp. 189-201.
[45] Sundstrom, O.; Guzzella, L., "A generic dynamic programming Matlab function," Control Applications, (CCA) & Intelligent Control, (ISIC), 2009 IEEE , vol., no., pp.1625,1630, 8-10 July 2009.
[46] Posada, F., Bedick, C., Clark, N., Kozlov, A. et al., "Low Temperature Combustion with Thermo-Chemical Recuperation," SAE Technical Paper 2007-01-4074, 2007.
[47] Lemmon, E. W., McLinden, M. O., & Huber, M. L. (2002). NIST Standard Reference Database 23-NIST Thermodynamic and Transport Properties REFPROP, Version 7.0 (No. World Wide Web-Internet and Web Information Systems).
[48] Kumar, U. and Karimi, M.N., 2014. Low grade Waste Heat Recovery for Optimized Energy Efficiencies and Enhanced Sustainability in Process Industries: A Comprehensive Review. International Journal of Multidisciplinary Sciences and Engineering, 5.
[49] Mansour, C.J., 2016. Trip-based optimization methodology for a rule-based energy management strategy using a global optimization routine: the case of the Prius plug-in hybrid electric

vehicle. Proceedings of the Institution of Mechanical Engineers, Part D: Journal of Automobile Engineering, 230(11), pp.1529-1545.